Fetal Dose Estimates for ^{18}F-Fluoro-L-Thymidine Using a Pregnant Monkey Model

Rachel M. Bartlett, Robert J. Nickles, Todd E. Barnhart, Bradley T. Christian, James E. Holden, and Onofre T. DeJesus

Department of Medical Physics, School of Medicine and Public Health, University of Wisconsin–Madison, Madison, Wisconsin

Estimating the radiation dose received by the fetus from nuclear medicine procedures is important because of the greater sensitivity of rapidly developing fetal tissues to ionizing radiation. ^{18}F-fluoro-L-thymidine (FLT) uptake is related to cellular proliferation and is currently used to monitor tumor progression and response to therapy. This study was undertaken to estimate—on the basis of biodistribution data obtained by PET/CT in pregnant rhesus monkeys—radiation absorbed dose to a human fetus administered ^{18}F-FLT. **Methods:** Three pregnant rhesus macaques (gestational age, 113 ± 8 d) were administered ^{18}F-FLT and imaged for 2 h on a PET/CT scanner. Time–activity curves for maternal and fetal organs were generated in anatomic regions of interest identified via CT. Doses were estimated using OLINDA/EXM and the 6-mo-pregnant human model. **Results:** The extrapolated whole-body maternal dose obtained, 11.4 μGy/MBq, is similar to the previously reported adult female dose of 15.6 μGy/MBq. The estimated total-body dose to a human fetus is 24 μGy/MBq. Significant long-term ^{18}F-FLT accumulation in fetal liver resulted in a fetal liver dose of 53 μGy/MBq. **Conclusion:** The fetal dose estimate in a 6-mo-pregnant human using ^{18}F-FLT is slightly greater than that reported for ^{18}F-FDG. ^{18}F-FLT trapping in the fetal liver should be considered in the risk–benefit analysis of ^{18}F-FLT PET examination in pregnant patients.

Key Words: ^{18}F-fluoro-L-thymidine (FLT); fetus; dosimetry

Estimating fetal radiation dose from nuclear medicine procedures is of considerable importance because rapidly developing fetal tissues are more sensitive to ionizing radiation. Radiopharmaceutical biokinetic data from pregnant women are very limited, primarily because of such concerns. Although the physical dosimetric aspects related to specific absorbed fractions can be mathematically modeled using realistic pregnant female phantoms (*1*), modeling the kinetics of radiopharmaceutical uptake, biodistribution, transfer, metabolism, and excretion in the fetus is complicated by its complex dependence on the tracer's maternal and fetal pharmacology (*2*). The pregnant nonhuman primate model is a reasonable approach previously used by Stabin to estimate ^{18}F-FDG fetal dose (*3*). The goal of this study was to estimate absorbed dose to a human fetus from ^{18}F-fluorothymidine (^{18}F-FLT) PET studies using biodistribution and pharmacokinetic data obtained in pregnant rhesus monkeys by PET/CT.

^{18}F-FLT is a PET agent with demonstrated utility in assessing tumor proliferation and response to therapy (*4,5*). ^{18}F-FLT has high specificity for thymidine kinase-1, whose activity increases 10-fold as cells enter the S phase (*5,6*). ^{18}F-FLT metabolic products are retained in cells at rates proportional to thymidine kinase-1 activities, making accumulation of ^{18}F-FLT an indirect marker of cellular proliferation. Establishing fetal radiation dose estimates in ^{18}F-FLT PET studies will allow rational risk-based decisions regarding the conduct of ^{18}F-FLT imaging of pregnant women.

MATERIALS AND METHODS

Radiopharmaceutical Preparation

^{18}F-FLT was prepared according to the method of Martin et al. (*7*). Briefly, 20 mg of 3-*N*-Boc-1-[5-*O*-(4,40-dimethoxytrityl)-3-*O*-nosyl-2-deoxy-β-D-lyxofuranosyl]thymine (ABX GmbH) in 500 μL of acetonitrile was reacted with azeotropically dried ^{18}F-fluoride-K222/KHCO$_3$. Deprotection for 5 min using 0.5 mL of 1N HCl at 110°C was done. After cooling, 1.5 mL of 2N sodium acetate was added and unreacted ^{18}F-fluoride was removed via an Alumina N cartridge (Waters). ^{18}F-FLT was purified by reverse-phase high-performance liquid chromatography (Alltech Econosil C18 10 μm, 250 × 10 mm, mobile phase = 90:10 water:ethanol). The ^{18}F-FLT peak was collected, made isotonic with saline, and sterilized through a 0.22-μm filter. The ^{18}F-FLT specific activity was 104 ± 30 GBq/μmol (2.8 ± 0.8 Ci/μmol).

Animal Subjects

Three healthy pregnant rhesus monkeys (Table 1) from the breeding colony of the Wisconsin National Primate Research Center were used in these studies. Fetal weights were estimated using the method of Digiacomo et al. (*8*). Animal care and use procedures for all experiments were approved by the University of Wisconsin–Madison Institutional Animal Care and Use Committee in compliance with National Institutes of Health regulations on research use of nonhuman primates. Wisconsin National Primate Research Center personnel experienced in the care of pregnant rhesus macaques transported the conscious animals between the housing facility and the University of Wisconsin Hospital PET/CT

TABLE 1. Characteristics of Experimental Subjects

Monkey	Body weight (kg)	Gestational day	Estimated fetal weight (g)*	Injected dose (MBq)
1	8.70	119/165	287	164.3
2	8.78	116/165	274	158.4
3	9.21	103/165	220	162.4

*Based on gestational age and placental and fetal weight formula reported by Digiacomo et al. (8) from sample of 209 full-term rhesus macaques with mean birth weight of 480 g.

suite. The animals were initially anesthetized with ketamine (15 mg/kg intramuscularly) and then were maintained on 1%−2% isoflurane during the PET study. Body temperature was controlled by loosely wrapping the animals with a forced-air warming device (Bair Hugger; Arizant Healthcare Inc.). The vital signs of the animals were monitored throughout the imaging session, and their uneventful recovery after the study was observed.

PET/CT Studies

Data were acquired on a Discovery LS PET/CT scanner (GE Healthcare) in 2-dimensional mode to maximize image resolution. The animals were oriented perpendicularly to the length of the scanner bed in a left lateral decubitus position allowing imaging of the fetus and all maternal organs in a single bed position. CT data were acquired at 120 kVp and 30 mA x-rays before PET. A dynamic PET sequence of 8 × 15 s, 6 × 30 s, 5 × 60 s, 5 × 120 s, 4 × 300 s, and 8 × 600 s for a total of 120 min was initiated on ^{18}F-FLT injection.

Given minimal ^{18}F-FLT uptake within heart tissue (9), a region of interest (ROI) was delineated over the maternal left ventricle to obtain time–activity blood curves. The limited blood sampling and metabolite analysis done was sufficient to characterize both metabolite formation and blood clearance (10,11).

Raw PET data were normalized and corrected for dead time, randoms, scatter, and attenuation. Images were reconstructed using an iterative ordered-subsets expectation maximization algorithm (4 iterations, 16 subsets) into a 256 × 256 (transverse) × 35 (axial) image matrix with 2.14 × 2.14 × 4.25 mm pixel size.

PET Image Analysis

Images were analyzed using the software package Amira 4.1 (Mercury Computer Systems). ROIs in the maternal kidney, liver, heart, marrow, and bladder and in the placenta and fetus were identified via CT and applied to the dynamic PET dataset to generate time–activity curves. The fetal ROI encompassed the entire uterine cavity enveloped by the placenta and included amniotic fluid. ROIs for bladder contents and organ volume were delineated by thresholding to exclude voxels below 5% of the maximum bladder value.

Tracer Kinetic Data Analysis

Each organ's measured activity concentration was corrected for recovery to reflect the true total injected activity in each frame (12). For the early frames (first 40 min) of the study, the measured fractional recovery was 0.71, which gradually increased to recoveries of 0.80–0.85 in the last 8 frames. Recovery-corrected radioactivity concentrations in CT-delineated monkey organ ROIs, expressed as percentage injected activity (MBq/MBq-g), were

plotted versus time to generate time–activity curves. Organ residence times were determined from the time–activity curves by adding the area under the curve for the 0- to 120-min time frame calculated using trapezoidal integration, to the integrated area from 120 min to infinity assuming clearance by physical decay only. The residence time in the remainder of the body is the summed residence times for all source organs subtracted from the fixed total body dose of $t_{1/2}/\ln 2 = 2.62$ h assuming no excretion.

Monkey data were extrapolated to human values using the following equation (13):

$$\left(\frac{\%ID}{g_{organ}} \times Body\,Weight\,(kg)\right)_{animal} \times \left(\frac{Organ\,Weight\,(g)}{Body\,Weight\,(kg)}\right)_{human} = \left(\frac{\%ID}{g_{organ}}\right)_{human},$$

where animal body weights were from Table 1 and human organ and body weights were from the standard 6-mo-pregnant female model. Bladder measurements involved no voiding, and the bladder content residence time was not scaled from animal to human.

Considering that the average rhesus monkey gestation period is 165 d (14), versus 270 d for humans, the mean gestation day for the monkeys of 113 ± 8 d extrapolates to 6.1 ± 0.5 mo in human gestational time. Thus, the 6-mo-pregnant 62-kg human model in the OLINDA/EXM software (Vanderbilt University) was used (15).

Fetal liver dose was estimated as the sum of self-dose and contributions from maternal organs. Fetal liver self-dose was evaluated using the method of Stabin et al. (16) and involved a 50-mL sphere to represent the estimated 49-g fetal liver in a 1,642-g human fetus (17). Dose from maternal organs was estimated using the method of Millard et al. (18).

RESULTS

Figure 1, the PET images of 1 pregnant animal, displays the average distribution of ^{18}F-FLT at early, mid, and late time frames. Rapid uptake in the maternal liver, maternal kidneys, placenta, and fetus is seen. Continuous bladder accumulation of ^{18}F is also seen since no voiding was involved. Typical time–activity curves for the main source organs—maternal kidneys, maternal liver, placenta, and fetus—are shown in Figure 2.

Human residence times for selected source organs extrapolated from each animal are presented in Table 2. OLINDA/EXM-generated individual and mean organ doses using these residence times are presented in Table 3. For comparison, values reported by Vessele et al. (19) are included in Table 3.

Another view of an animal's abdominal area (Fig. 3A) shows the fetus and placenta. Closer inspection of ^{18}F-FLT uptake in the fetus in Figure 1 shows increasing ^{18}F-FLT accumulation in the fetal liver that leveled off an hour after injection (Fig. 3B). In contrast, continuous clearance is seen in the maternal liver (Figs. 1 and 2). Calculated individual and mean self-dose and total fetal liver doses are listed in Table 4.

DISCUSSION

Although the risks posed to the fetus by most nuclear medicine procedures are minimal based on deterministic
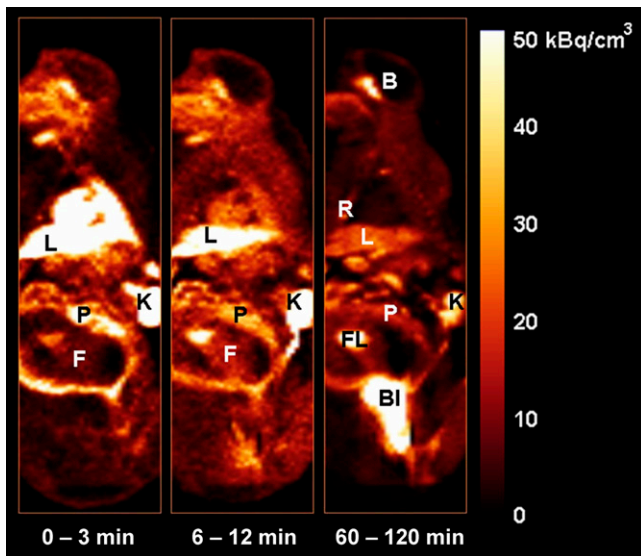
FIGURE 1. Coronal images of pregnant monkey displaying average tracer distribution over early (0–3 min, first 10 frames), mid (6–12 min, 5 frames), and late (60–120 min, last 6 frames) time frames. B = brain; Bl = bladder; F = fetus; FL = fetal liver; K = kidney; L = liver; P = placenta; R = ribs.

TABLE 2. Extrapolated Human Residence Times in Selected Source Organs

Organ	Residence time (h)			
	Monkey 1	Monkey 2	Monkey 3	Mean ± SD
Kidneys	0.046	0.053	0.084	0.061 ± 0.020
Liver	0.114	0.102	0.110	0.108 ± 0.006
Heart	0.008	0.006	0.008	0.007 ± 0.001
Marrow	0.107	0.181	0.079	0.122 ± 0.052
Bladder	1.28	1.25	1.38	1.30 ± 0.070
Placenta	0.013	0.016	0.013	0.014 ± 0.002
Fetus	0.059	0.065	0.059	0.061 ± 0.004
Remainder of body	0.994	0.952	0.887	0.944 ± 0.054

and stochastic considerations (20), there remains a need to estimate dose delivered to the biologically sensitive embryo or fetus from new diagnostic nuclear imaging procedures. Dose estimates have relied mostly on small-animal data, notably guinea pigs, rabbits, and rodents, because of a paucity of available human data on placental and fetal uptake of radiopharmaceuticals (21). Extrapolation of small-animal data to humans has several limitations, in-
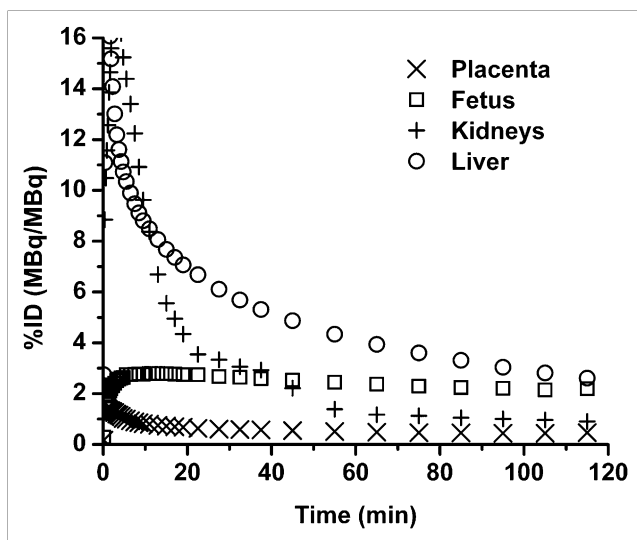

FIGURE 2. Average time–activity curves (n = 3) extrapolated to 62-kg pregnant human model, normalized for injected dose and organ weight for maternal kidneys, liver, placenta, and fetus.

cluding shorter gestation periods, the presence of multiple fetuses and, in general, various unspecified and undetermined species differences. A reasonable animal model to use in human fetal dosimetry is the pregnant nonhuman primate.

The use of PET to study pregnant monkeys was first reported by Lindberg et al. (22). Other PET studies reported on maternal–fetal transfers of opioids (23) and amino acids (24) and on placental blood volume (25). PET/MRI studies of pregnant monkeys to assess maternal–fetal transfer of ^{18}F-FDG (26) and cocaine (27) have also been reported. Another application of PET in pregnant monkeys is in assessing fetal uptake of environmental chemicals to establish the role of in utero fetal exposure in adult disease (28,29).

PET data from pregnant monkeys were first used to estimate fetal dose for the common PET agent, ^{18}F-FDG (3). This current study assessed fetal dose for the PET agent ^{18}F-FLT to define radiation risk associated with its use in pregnant women. Standard assumptions made in the calculations are that distribution of tracer in source organs is uniform and that tracer loss after data acquisition occurs only by physical decay, a conservative assumption expected to overestimate the calculated radiation exposure. The calculations also involved no voiding, to represent a worst-case scenario since the maternal bladder was the main contributor to fetal dose. As a result, the dose to the maternal urinary bladder wall was about an order of magnitude higher than that reported by Vessele et al. (19). Properly timed voiding is known to significantly reduce bladder dose (30,31) and, consequently, will also reduce fetal dose. Except for bladder dose, our human organ dose estimates (Table 3) are on the same order as or lower than those reported by Vessele et al. (19).

With the human fetal dose of 24 μGy/MBq, a 185-MBq (5-mCi) ^{18}F-FLT injection yields an estimated fetal dose of 4.4 mSv (4.4 mGy), significantly below the threshold of 50 mSv (50 mGy) recommended by the National Council on Radiation Protection and Measurements (32). It is noteworthy that the dose to the uterus approximates that to the whole fetus (Table 3).

Organ	Dose estimate (μSv/MBq or μGy/MBq)				
	Monkey 1	Monkey 2	Monkey 3	Mean ± SD	Vessele et al.*
Adrenals	10.3	10.2	10.4	10.3 ± 0.1	20.1
Brain	5.64	5.34	4.98	5.32 ± 0.33	5.07
Breasts	5.8	5.38	5.27	5.48 ± 0.28	7.23
Gallbladder wall	11.6	11.2	11.7	11.5 ± 0.3	19.6
LLI wall	19.0	18.4	19.3	18.9 ± 0.5	16.2
Small intestine	11.4	11.2	11.3	11.3 ± 0.1	18.6
Stomach wall	8.45	7.99	8.06	8.17 ± 0.25	14.9
ULI wall	10.0	9.62	9.78	9.80 ± 0.19	14.0
Heart wall	9.36	8.51	8.74	8.87 ± 0.44	22.3
Kidneys	35.8	40.5	60.5	45.6 ± 13.1	42.0
Liver	22.5	20.5	21.8	21.6 ± 1.0	64.2
Lungs	7.2	6.77	6.56	6.84 ± 0.33	12.6
Muscle	10.5	10.0	10.2	10.2 ± 0.3	23.7
Ovaries	15.0	15.0	14.7	14.9 ± 0.2	20.7
Pancreas	9.99	9.55	9.75	9.76 ± 0.22	19.6
Red marrow	15.0	19.5	12.9	15.8 ± 3.4	33.0
Skin	7.04	6.64	6.72	6.8 ± 0.2	5.07
Spleen	8.58	8.23	8.65	8.49 ± 0.23	28.9
Thymus	6.74	6.24	6.06	6.36 ± 0.35	13.5
Thyroid	6.04	5.62	5.37	5.68 ± 0.34	12.7
Urinary bladder wall	1.1×10^3	1.1×10^3	1.2×10^3	$1.1 \times 10^3 \pm 0.06$	0.174×10^3
Uterus	22.3	21.8	22.9	22.3 ± 0.55	25.3
Fetus	23.5	24.2	24.4	24.0 ± 0.5	—
Placenta	14.9	16.8	15.6	15.8 ± 1.0	—
Total body	11.6	11.3	11.4	11.4 ± 0.15	15.6

*Estimated mean organ dose for woman who voids at 6 h after ^{18}F-FLT injection (19).
LLI = lower large intestine; ULI = upper large intestine.

The average fetal ^{18}F-FLT residence time, 0.061 ± 0.004 h, is similar to that reported for ^{18}F-FDG in the 6-mo-pregnant human, 0.064 h (3). The ^{18}F-FLT fetal dose estimate is, however, higher than that for ^{18}F-FDG, 0.024 mGy/MBq vs. 0.017 mGy/MBq, likely because of the difference in bladder content dose contributions (no bladder voiding vs. voiding at 4 h).

Another difference observed was the continuous ^{18}F-FLT clearance from maternal liver (Figs. 1 and 2), compared with the uptake and retention of ^{18}F-FLT in the fetal liver (Figs. 1 and 3B). The significant accumulation of ^{18}F-FLT observed in the maternal ribs and spine (Fig. 1) is expected since the bone marrow is the primary site of hematopoiesis (33). In the fetus, the liver is the major site of hematopoi-

esis, with the full hematopoiesis transition from liver to marrow occurring after birth (34). Furthermore, approximately 70%−80% of umbilical blood enters the fetus through the fetal liver before distribution by the fetal heart to other fetal tissues (35). These 2 mechanisms likely underlie the observed trapping of ^{18}F-FLT in fetal liver.

Using estimated monkey fetal weights (Table 1) and estimated liver and body weights of 49 g and 1,642 g, respectively, for a human 6-mo fetus (17), we calculated a total radiation dose to the human fetal liver of 53 ± 0.9 μGy/MBq (196 mrad/mCi) (Table 4), or approximately 9.8 mGy (980 mrad) for a 185-MBq (5-mCi) injection. Although much below the 5- to 10-cGy suggested threshold for fatal and nonfatal malformations or defects in the embryo or
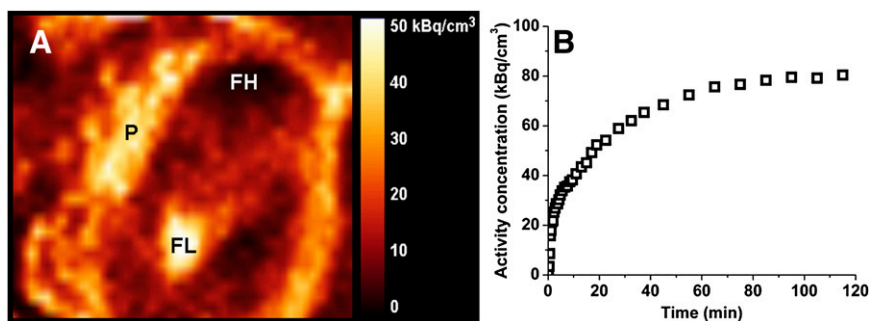

FIGURE 3. (A) PET/CT image of abdominal region of pregnant monkey showing placenta (P), fetal head (FH), and liver (FL). (B) Time–activity curve for fetal liver.

TABLE 4. Individual and Mean Fetal Liver Doses (Extrapolated to Humans)

Dose (μGy/MBq)	Monkey 1	Monkey 2	Monkey 3	Mean dose ± SD
Self	45	30	27	34 ± 10
Total	64	49	47	53 ± 9

fetus, a genetic disease risk estimated to be 0.01%−0.09% per 10 mGy (*20*) is worthy of careful consideration.

CONCLUSION

Using the pregnant rhesus macaque model, we found that a single 185-MBq (5-mCi) ^{18}F-FLT study gives the 6-mo fetus an estimated dose of 4.4 mSv (4.4 mGy), comparable to common nuclear medicine radiopharmaceuticals. Higher ^{18}F-FLT uptake and retention were observed in the fetal liver than in the maternal liver—likely because of their different roles in hematopoiesis—and resulted in an estimated fetal liver dose of 9.8 mGy (980 mrad) for a 185-MBq (5-mCi) ^{18}F-FLT injection. The probability of genetic liver disease from this dose should be considered in risk–benefit analyses of ^{18}F-FLT PET examinations in pregnant patients. PET studies using the pregnant monkey model are useful in assessing maternal–fetal transfer of radiotracers to obtain dosimetric data to guide nuclear medicine applications in pregnant women.

REFERENCES

1. Shi CY, Xu XG, Stabin MG. SAF values for internal photon emitters calculated for the RPI-P pregnant-female models using Monte Carlo methods. *Med Phys.* 2008;35:3215–3224.
2. Vicini P, Brill AB, Stabin MG, Rescigno A. Kinetic modeling in support of radionuclide dose assessment. *Semin Nucl Med.* 2008;38:335–346.
3. Stabin MG. Proposed addendum to previously published fetal dose estimate tables for ^{18}F-FDG. *J Nucl Med.* 2004;45:634–635.
4. Mankoff DA, Shields AF, Krohn KA. PET imaging of cellular proliferation. *Radiol Clin North Am.* 2005;43:153–167.
5. Bading JR, Shields AF. Imaging of cell proliferation: status and prospects. *J Nucl Med.* 2008;49(suppl 2):64S–80S.
6. Sherley JL, Kelly TJ. Regulation of human thymidine kinase during the cell cycle. *J Biol Chem.* 1988;263:8350–8358.
7. Martin SJ, Eisenbarth JA, Wagner-Utermann U, et al. A new precursor for the radiosynthesis of [18]FLT. *Nucl Med Biol.* 2002;29:263–273.
8. Digiacomo RF, Shaughnessy PW, Tomlin SL. Fetal-placental weight relationships in the rhesus (*Macaca mulatta*). *Biol Reprod.* 1978;18:749–753.
9. Jansson O, Bohman C, Munch-Petersen B, Eriksson S. Mammalian thymidine kinase 2: direct photoaffinity labeling with [32P]dTTP of the enzyme from spleen, liver, heart and brain. *Eur J Biochem.* 1992;206:485–490.
10. Reishcl G, Blocher A, Rongqing W, et al. Simplified, automated synthesis of 3′[18]fluoro-3′-deoxy-thymidine ([18]FLT) and simple method for metabolite analysis in plasma. *Radiochimica Acta.* 2006;94:447–451.
11. Shields AF, Briston DA, Chandupatla S, et al. A simplified analysis of [18]F3′-deoxy-3′-fluorothymidine metabolism and retention. *Eur J Nucl Med Mol Imaging.* 2005;32:1269–1275.
12. Brown AK, Fujita M, Fujimura Y, et al. Radiation dosimetry and biodistribution in monkey and man of ^{11}C-PBR28: a PET radioligand to image inflammation. *J Nucl Med.* 2007;48:2072–2079.
13. Kirschner AS, Ice RD, Beierwaltes WH. Radiation dosimetry of [131]I-19-iodocholesterol. *J Nucl Med.* 1973;14:713–717.
14. Newell-Morris L, Fahrenbruch C. Practical and evolutionary considerations for use of the nonhuman primate model in prenatal research. In: Watts E, ed. *Nonhuman Primate Models for Human Growth and Development.* A.R. Liss; 1985:9–40.
15. Stabin MG, Sparks RB, Crowe E. OLINDA/EXM: the second-generation personal computer software for internal dose assessment in nuclear medicine. *J Nucl Med.* 2005;46:1023–1027.
16. Stabin MG, Stubbs JB, Russell JR. Review of the fetal radiation doses received from ^{59}Fe kinetic studies at Vanderbilt University in the 1940's. *Health Phys.* 1997;72:701–707.
17. Gimondo P, Mirk P, La Bella A, Messina G, Pizzi C. Sonographic estimation of fetal liver weight: an additional biometric parameter for assessment of fetal growth. *J Ultrasound Med.* 1995;14:327–333.
18. Millard RK, Saunders M, Palmer AM, Preece AW. Approximate distribution of dose among foetal organs for radioiodine uptake via placenta transfer. *Phys Med Biol.* 2001;46:2773–2783.
19. Vesselle H, Grierson J, Peterson LM, Muzi M, Mankoff DA, Krohn KA. ^{18}F-fluorothymidine radiation dosimetry in human PET imaging studies. *J Nucl Med.* 2003;44:1482–1488.
20. Steenvoorde P, Pauwels EK, Harding LK, Bourguignon M, Mariere B, Broerse JJ. Diagnostic nuclear medicine and risk for the fetus. *Eur J Nucl Med.* 1998; 25:193–199.
21. Russell JR, Stabin MG, Sparks RB. Placental transfer of radiopharmaceuticals and dosimetry in pregnancy. *Health Phys.* 1997;73:747–755.
22. Lindberg BS, Hartvig P, Lilja A, et al. Positron-emission tomography: a new approach to feto-maternal pharmacokinetics. *NIDA Res Monogr.* 1985;60: 88–97.
23. Hartvig P, Lindberg BS, Lilja A, Lundqvist H, Langstrom B, Rane A. Positron emission tomography in studies on fetomaternal disposition of opioids. *Dev Pharmacol Ther.* 1989;12:74–80.
24. Berglund L, Andersson J, Lilja A, et al. Amino acid transport across the placenta measured by positron emission tomography and analyzed by compartment modelling. *J Perinat Med.* 1990;18:89–100.
25. Berglund L, Lilja A, Andersson J, et al. Maternal blood volume in placenta of the rhesus monkey measured in vivo by positron emission tomography. *Gynecol Obstet Invest.* 1991;31:1–7.
26. Benveniste H, Fowler JS, Rooney WD, et al. Maternal-fetal in vivo imaging: a combined PET and MRI study. *J Nucl Med.* 2003;44:1522–1530.
27. Benveniste H, Fowler JS, Rooney W, et al. Maternal and fetal ^{11}C-cocaine uptake and kinetics measured in vivo by combined PET and MRI in pregnant nonhuman primates. *J Nucl Med.* 2005;46:312–320.
28. DeJesus OT, Flores LG, Converse AK, et al. Assessing environmental chemical uptake in fetal brain in utero: a preliminary PET/CT study. *J Radioanal Nucl Chem.* 2006;269:561–564.
29. Bartlett RM, Nickles RJ, Murali D, et al. Paraquat uptake in adult and fetal macaque brain in vivo: a PET study [abstract]. *Turku PET Symposium Book of Abstracts.* 2008:15. Available at: http:pet.utu.fi/files/PET2008_book_of_abstracts.pdf. Accessed November 5, 2009.
30. Dowd MT, Chen CT, Wendel MJ, Faulhaber PJ, Cooper MD. Radiation dose to the bladder wall from 2-[18]fluoro-2-deoxy-D-glucose in adult humans. *J Nucl Med.* 1991;32:707–712.
31. Thomas SR, Stabin MG, Chen CT, Samaratunga RC. MIRD pamphlet no. 14: a dynamic urinary bladder model for radiation dose calculations. *J Nucl Med.* 2002;33:783–802.
32. National Council on Radiation Protection and Measurements. *Considerations Regarding the Unintended Radiation Exposure of the Embryo, Fetus or Nursing Child.* Bethesda, MD: NCRP Publications; 1994. NCRP commentary no. 9.
33. Shields AF, Grierson JR, Dohmen BM, et al. Imaging proliferation in vivo with [F-18]FLT and positron emission tomography. *Nat Med.* 1998;4:1334–1336.
34. Blackburn ST. *Maternal, Fetal, & Neonatal Physiology: A Clinical Perspective.* 3rd ed. St. Louis, MO: Saunders (Elsevier Health Sciences); 2007:243–244.
35. Kiserud T, Rasmussen S, Skulstad SM. Blood flow and degree of shunting through the ductus venosus in the human fetus. *Am J Obstet Gynecol.* 2000;182:147–153.